

Video Article

Melt Electrospinning Writing of Three-dimensional Poly(ϵ -caprolactone) Scaffolds with Controllable Morphologies for Tissue Engineering Applications

Felix M. Wunner¹, Onur Bas¹, Navid T. Saidy¹, Paul D. Dalton², Elena M. De-Juan Pardo¹, Dietmar W. Hutmacher^{1,3,4}¹ARC ITTC in Additive Biomanufacturing, Institute for Health and Biomedical Innovation (IHBI), Queensland University of Technology (QUT)²Department for Functional Materials in Medicine and Dentistry and Bavarian Polymer Institute, University of Würzburg³Institute for Advanced Study, Technical University of Munich (TUM)⁴George W Woodruff School of Mechanical Engineering, Georgia Institute of TechnologyCorrespondence to: Dietmar W. Hutmacher at dietmar.hutmacher@qut.edu.auURL: <https://www.jove.com/video/56289>DOI: [doi:10.3791/56289](https://doi.org/10.3791/56289)Keywords: Bioengineering, Issue 130, melt electrospinning writing, additive manufacturing: bio-manufacturing, direct writing: tissue engineering & regenerative medicine, poly(ϵ -caprolactone), product development, medical product development, 3D printing

Date Published: 12/23/2017

Citation: Wunner, F.M., Bas, O., Saidy, N.T., Dalton, P.D., Pardo, E.M., Hutmacher, D.W. Melt Electrospinning Writing of Three-dimensional Poly(ϵ -caprolactone) Scaffolds with Controllable Morphologies for Tissue Engineering Applications. *J. Vis. Exp.* (130), e56289, doi:10.3791/56289 (2017).

Abstract

This tutorial reflects on the fundamental principles and guidelines for electrospinning writing with polymer melts, an additive manufacturing technology with great potential for biomedical applications. The technique facilitates the direct deposition of biocompatible polymer fibers to fabricate well-ordered scaffolds in the sub-micron to micro scale range. The establishment of a stable, viscoelastic, polymer jet between a spinneret and a collector is achieved using an applied voltage and can be direct-written. A significant benefit of a typical porous scaffold is a high surface-to-volume ratio which provides increased effective adhesion sites for cell attachment and growth. Controlling the printing process by fine-tuning the system parameters enables high reproducibility in the quality of the printed scaffolds. It also provides a flexible manufacturing platform for users to tailor the morphological structures of the scaffolds to their specific requirements. For this purpose, we present a protocol to obtain different fiber diameters using melt electrospinning writing (MEW) with a guided amendment of the parameters, including flow rate, voltage and collection speed. Furthermore, we demonstrate how to optimize the jet, discuss often experienced technical challenges, explain troubleshooting techniques and showcase a wide range of printable scaffold architectures.

Video Link

The video component of this article can be found at <https://www.jove.com/video/56289/>

Introduction

The manufacture of three-dimensional (3D) biocompatible structures for cells is one of the key contributions of additive biomanufacturing to tissue engineering (TE), aiming to restore tissues by applying customized biomaterials, cells, biochemical factors, or a combination of them. Therefore, the main requirements of scaffolds for TE applications include: manufacturability from biocompatible materials, controllable morphological properties for targeted cell invasion and optimized surface properties for enhanced cell interaction¹.

MEW is a solvent-free manufacturing technique that combines the principles of additive manufacturing (often called 3D printing) and electrospinning for the production of polymeric meshes with highly ordered ultrathin fiber morphologies². It is a direct writing approach and accurately deposits fibers according to preprogrammed codes³, referred to as G-Codes. Melt electrospun constructs are currently prepared using a flat^{4,5} or a mandrel^{6,7} collector to fabricate porous flat and tubular scaffolds, respectively.

This technique offers significant benefits to the TE and regenerative medicine (RM) community due to the possibility to directly print medical-grade polymers, such as poly(ϵ -caprolactone) (PCL), which presents excellent biocompatibility⁸. Other advantages are the possibility to customize the size and distribution of the porosity, by depositing the fibers in a highly-organized manner to fabricate scaffolds of high surface-to-volume ratios. Before MEW can be performed, the polymer first requires the application of heat⁹. Once in a fluid state, an applied air pressure forces it to flow out through a metallic spinneret that is connected to a high voltage source. The force balance between the surface tension and the attraction of the electrostatically charged droplet to the grounded collector leads to the formation of a Taylor cone followed by the ejection of a jet¹⁰.

Images and a schematic drawing of the in-house build MEW device used for this protocol are shown in **Figure 1**. It additionally demonstrates the principles of using insulating tape to avoid electrical discharge between the heating elements and the electrically charged brass part surrounding the spinneret. Insufficient insulation would lead to internal damage of the implemented hardware.

Depending on the adjustment of the three system parameters (temperature, collection speed and air pressure), MEW enables the fabrication of fibers with different diameters, explained in the discussion section. In most cases, however, fine-tuning and optimization of the jet will be required before a stable jet will be ejected. The visualization of the electrified travelling jet is an effective way to verify the consistency and homogeneity

of the process. In an ideal case, the flight path resembles a catenary curve acquired as a result of a force balance controlled by the system parameters¹¹. Further, the micro- and macro-structure of the scaffolds is dependent on the flight path of the polymer jet¹². A detailed table of different deflection behaviors and measures for optimization is given in the discussion section.

In the present study, we present a protocol that describes the fabrication steps for the manufacture of highly controlled fibrous scaffolds using MEW technology. In this work, medical grade PCL (molecular weight 95-140 kg/mol) was used, as this medical grade PCL has improved purity over technical grade, and its mechanical and processing properties are excellent for MEW. Broad melt processing range of PCL originates from its low melting point (60 °C) and high thermal stability. Moreover, PCL is a slow-rate biodegradable polymer, which makes it an excellent material for many tissue engineering applications¹³.

For this study, the temperature and collector distance will be kept constant (65 °C and 82 °C for the syringe and spinneret temperatures (respectively) and 12 mm for the collector distance); applied voltage, collector speed and air pressure, however, will be varied to fabricate fibers with targeted diameters. A detailed list of published studies using MEW scaffolds is provided in the results section and reveals different applications for the fields of TE and RM (**Table 1**).

Protocol

1. Material Preparation

1. Fill 2 g of PCL in a 3 mL plastic syringe with a funnel and insert a piston into the open end.
2. Place the syringe in a preheated oven at 65 °C for 8 h. Point the tip upwards to allow the air bubbles to aggregate close to the opening.
3. Push the piston with a thin object to release the trapped air within the molten material.
4. Let it cool down to room temperature, which is achieved when the polymer is not transparent anymore after 10 minutes.
5. Store the PCL pre-loaded syringe at room temperature in a dry and dark environment until it is used.

2. Hardware and Software Setup

1. Attach a 23G flat tipped needle (spinneret) to the syringe and a barrel adapter at the other end to connect the syringe to the air pressure system.
2. Place the syringe in the print head and press it down until the spinneret tip stands out 1 mm from the brass part on the bottom side of the head.
3. Mount a collector on the stage and clean the surface as well as the print head with 70% (vol/vol) ethanol to remove dust or residual polymer.
4. Set the working distance by positioning a 12 mm high object between the spinneret and the collector and lower the print head until the spinneret tip just touches it.
5. Adjust the temperature regulators at the electrical box to 82 °C and 65 °C for the spinneret region and the syringe, respectively and power them on to melt the PCL.
6. Wait for at least 10 min until the polymer is molten and initiate the air pressure by setting the regulator to 1.8 bar.
7. Prepare the G-Code to define the size and shape, inter-filament distance and the number of layers of the scaffold and the collection speed of the process.
NOTE: A detailed template for fabricating flat and tubular scaffolds is provided in the discussion chapter (**Table 2**).
8. Double-check manually that all ground cables are connected securely to the enclosure and the wall plug.
9. Start the software (e.g., MACH 3) on the computer and upload the prepared G-code.

3. Scaffold fabrication

1. Close the front door of the enclosure, which connects the safety interlock and triggers the high voltage supply to the spinneret.
NOTE: Once the door is opened, for example when a print is finished or in case of an emergency, the high voltage drops and the scaffold can be removed safely.
2. Increase the high voltage gradually in 0.2 kV steps until a Taylor cone is formed and a fiber is ejected towards the collector (see exemplary Taylor cone in **Figure 1D**).
3. Allow the polymer melt to be extruded on the still collector plate to stabilize the jet without movement for 5 minutes. Remove the pile of material before commencing a new print.
4. Use the cursors on the keyboard to move the print head above the point where the G-codes will start.
5. Start the G-Code in the software on the computer.

4. Fiber Diameter Adjustment

1. Keep the working distance (12 mm) and the temperature regulators (82 °C and 65 °C for the spinneret region and the syringe, respectively) on a constant level, as described before in steps 2.4 and 2.5.
NOTE: A summary of adjusting different diameters is given in **Table 3**.
2. Print fibers with small sized diameters (3-10 µm). Reduce the air pressure level to 0.8 bar, adjust the applied voltage to 8 kV and set the collector speed to 1700 mm/min.
3. Print fibers with medium sized diameters (10-20 µm). Adjust the air pressure level to 1.5 bar, set voltage to 11 kV and lower the collection speed to 1200 mm/min.
4. Print fibers with large diameters (20-30 µm). Increase the air pressure level to 2.6 bar, alter the applied voltage to 12 kV and decrease the collection speed to 700 mm/min.

5. Jet Optimization

1. Illuminate the jet with a strong LED light from outside the enclosure for improved visibility.
2. Observe the behavior of the fiber for 1 minute and adjust the system parameters to optimize the process in small steps, *i.e.* 0.1 kV for applied voltage, 100 mm/min for collection speed and 0.1 bar for air pressure.

NOTE: A summary is given in **Table 4**.

3. Stabilize periodically deflecting behavior by decreasing the air-pressure, increasing the speed and minimizing the voltage until the flight path of the fiber resembles a stable catenary curve for more than 3 minutes.
4. Correct the flight path of a lagging behind jet by increasing the voltage, reducing the air pressure and reducing the speed of the collector. Apply those measures until the flight path of the fiber moves back to a catenary curve shape.
5. Avoid fibers travelling vertically towards the collector by decreasing the applied voltage, increasing the speed of the collector and increasing the air pressure until the flight path of the jet retains the shape of a catenary curve again.

6. Scaffold Collection

1. Open the door when the print is finished and use the cursor to move the collector plate towards the door for better accessibility.
2. Spray the scaffold with ethanol 70% (vol/vol) mix and wait 10 seconds until it visibly detaches from the collector.
3. Collect the finished scaffold by grabbing one edge with tweezers and lifting it out of the enclosure.

7. Troubleshooting

1. Decrease the applied voltage or open the door immediately if there is a spark between the spinneret visible or a cracking noise audible.
2. Remove all hazardous materials and liquids such as ethanol 70% (vol/vol) from the inside of the enclosure as a fire might ignite in case of potential sparking.
3. Program the G-Code accordingly that the spinneret moves away from the area where the scaffold is printed after all layers are done. This avoids material accumulation above the point where the spinneret finally stops.
4. Check the spinneret under a magnifier and verify that there is no damage to the spinneret as this will significantly influence the homogeneity of the Taylor cone.

Representative Results

Two different methods of collection are commonly used in MEW, which are flat collection and mandrel collection. The resulting architectures depend on the programming of the G-Code (**Table 2**), which is executed by the software.

Flat collection

Applying flat collectors refers to the most common method and facilitates the direct deposition of material referring to the pre-programmed G-code. 0/90 and 0/60 structures of different sizes are widely reported in literature. Furthermore, the capability of directly depositing molten fibers on the collector also facilitates the production of randomly yet organized structures when a patterned flat collector is used instead of a smooth one¹⁴.

Tubular

There is a great demand for the manufacture of scaffolds with tubular architectures for TE applications. MEW is an effective method to achieve tubular scaffolds with customized porosity by utilizing cylindrical collectors. These rotate along their own axis, while translating along the axis of the mandrel. Through fine tuning of the G-Code, the rotational as well as the translational speed is determined and the orientation of the fibers can be customized. Higher rotational speeds than translational speeds lead to radially orientated pores and vice versa. The total number of layers, distribution and morphology of the porosity will configure the mechanical properties of the scaffold. The inner diameter of the tubular scaffold will be determined by the external diameter of the implemented mandrel.

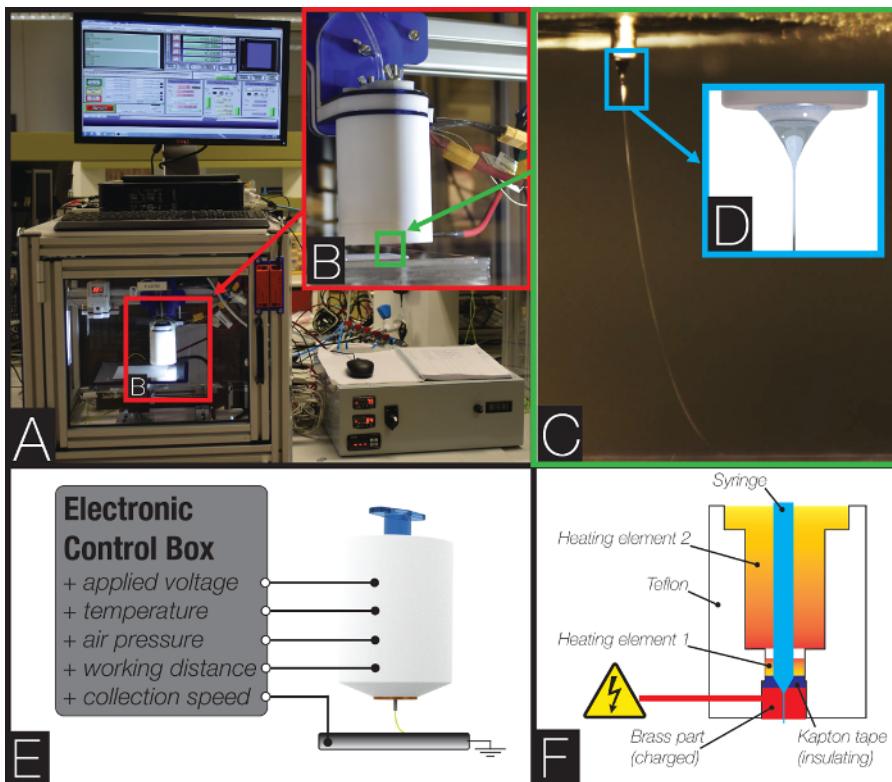


Figure 1: MEW setup. (A) including a PC, the printing unit and the electrical control box (B) the head and the collector (C) the fiber in a perfectly balanced flight phase and (D) a schematic illustration of a Taylor cone. (E) shows a schematic of a printer and lists the five most prevailing system parameters, including "applied voltage" (High Voltage Generator), "temperature" (Temperature Controller), "air pressure" (Pressure Regulator), "working distance" (adjustment via in-house designed movable z-axis) and "collection speed" (X and Y positioning slides). (F) demonstrates the design of the insulation system within the print head via a heat resistant polyamide tape. This prevents arcing between the "heating element 1" and the charged "Brass part". [Please click here to view a larger version of this figure.](#)

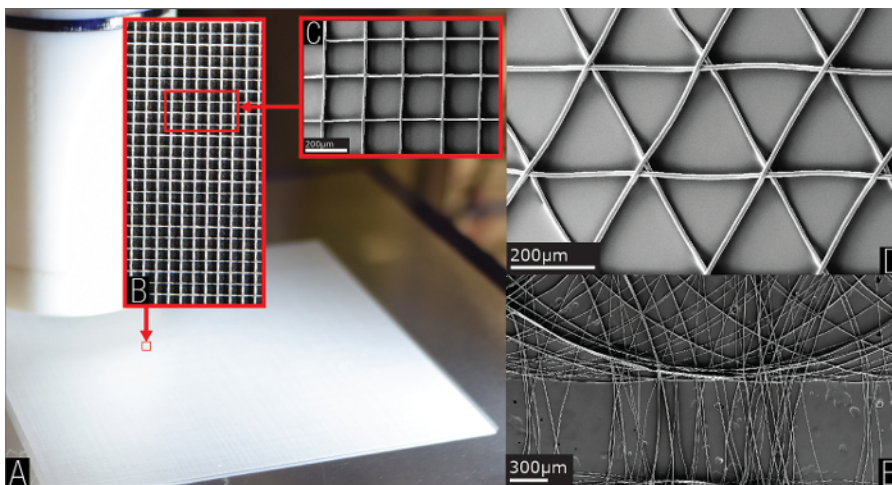


Figure 2: Different scaffolds fabricated with a flat collector (A), 0/90 lattice (B) and the same lattice in greater resolution (C). (D) demonstrates a 0/60 structure and (E) a randomly controlled structure. [Please click here to view a larger version of this figure.](#)

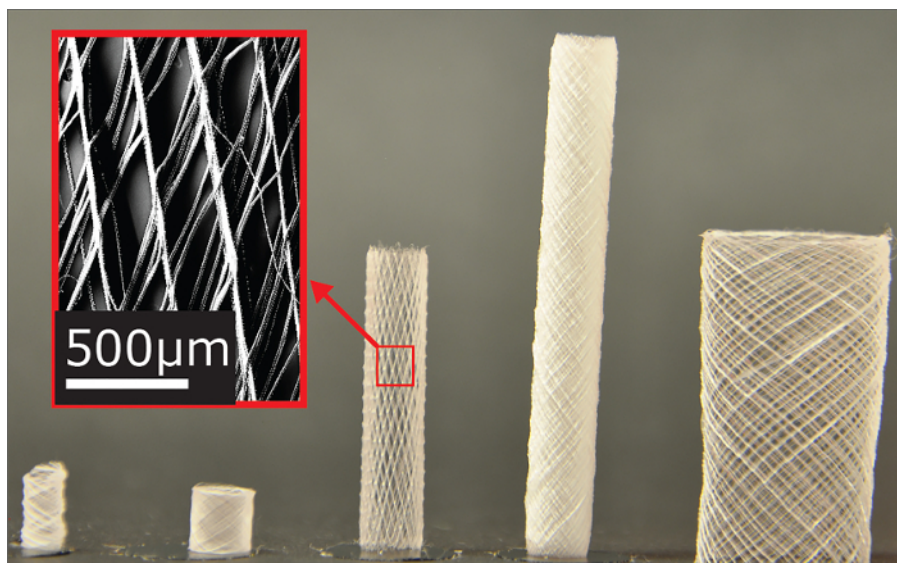


Figure 3: Showcasing of different tubular scaffolds and one respective representative image from scanning electron microscopy (SEM). [Please click here to view a larger version of this figure.](#)

Dermal fibroblast infiltration of poly(ϵ -caprolactone) scaffolds fabricated by melt electrospinning in a direct writing mode (Farrugia et al., 2013) ⁴ FLAT
Dermal fibroblast seeded PCL MEW scaffolds are evaluated for cell infiltration.
A tissue-engineered humanized xenograft model of human breast cancer metastasis to bone (Thibaudeau et al., 2014) ¹⁵ TUBULAR
Tubular MEW scaffolds are used to create a viable ectopic 'organ' bone in a mouse model to study human breast cancer metastasis to bone.
Species-specific homing mechanisms of human prostate cancer metastasis in tissue engineered bone (Holzapfel et al., 2014) ¹⁶ TUBULAR
MEW scaffolds are used to create a tissue engineered bone for prostate cancer research.
Enhancing structural integrity of hydrogels by using highly organised melt electrospun fibre constructs (Bas et al., 2015) ¹⁷ FLAT
MEW scaffolds with different lay-down patterns and poresizes are used to enhance the mechanical functionality of soft hydrogels.
Reinforcement of hydrogels using three-dimensionally printed microfibrils (Visser et al., 2015) ¹⁸ FLAT
Soft gelatin-based hydrogels are reinforced with MEW PCL scaffolds.
Melt electrospinning onto cylinders: effects of rotational velocity and collector diameter on morphology of tubular structures (Jungst et al., 2015) ⁶ TUBULAR
The influence of the translational and rotational speeds on the final morphology of tubular MEW scaffolds are systematically investigated.
Hierarchically structured porous poly(2-oxazoline) hydrogels (Haigh et al., 2016) ¹⁹ FLAT
MEW scaffolds are used as a sacrificial template to create a hierarchical 3D porosity network within a hydrogel.
A validated preclinical animal model for primary bone tumor research (Wagner et al., 2016) ²⁰ TUBULAR
MEW scaffolds are used to create humanized tissue engineered constructs for preclinical research on primary bone tumors.
Periosteum tissue engineering in an orthotopic in vivo platform (Baldwin et al., 2017) ²¹ TUBULAR
A multiphasic scaffold consisting of a MEW mesh and a hydrogel is developed for periosteum tissue regeneration applications.
Dimensional metrology of cell-matrix interactions in 3D microscale fibrous substrates (Tourlomousis and Chang, 2017) ²² FLAT
Cell-matrix interactions are investigated on MEW scaffolds with different architectures.
Endosteal-like extracellular matrix expression on melt electrospun written scaffold (Muerza-Cascante et al., 2017) ²³ FLAT
MEW PCL scaffolds are used to develop an endosteal bone-like tissue that promotes the growth of primary human haematopoietic stem cells.
3D printed lattices as an activation and expansion platform for T cell therapy (Delalat et al., 2017) ²⁴ FLAT
Scaffolds with different fiber spacing (200 μm, 500 μm and 1000 μm) are surface functionalised and seeded with T cells for expansion.
Biofabricated soft network composites for cartilage tissue engineering (Bas et al., 2017) ²⁵ FLAT
Biomimetic soft network composites consisting of a hydrogel matrix and reinforcing MEW meshes designed for articular cartilage repair are reported.
Via precise interface engineering towards bioinspired composites with improved 3D printing processability and mechanical properties (Hansske et al., 2017) ²⁶ FLAT
Magnesium fluoride nanoparticle reinforced PCL scaffolds fabricated by means of MEW are designed and developed for bone tissue engineering applications.

Table 1: References to a list of studies, in which MEW scaffolds were fabricated and used for biological applications. The list provides results of implemented flat as well as tubular scaffolds.

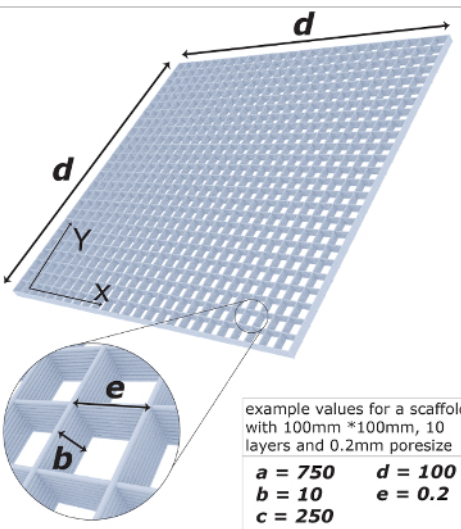
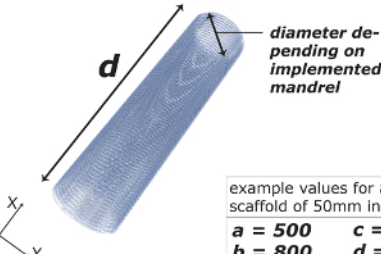
CODE	EXPLANATION	ILLUSTRATION						
G17 G21 G40 G49 G54 G80 G94	START OF PROGRAM	 <p>example values for a scaffold with 100mm *100mm, 10 layers and 0.2mm poresize</p> <table border="1"> <tr> <td>$a = 750$</td> <td>$d = 100$</td> </tr> <tr> <td>$b = 10$</td> <td>$e = 0.2$</td> </tr> <tr> <td>$c = 250$</td> <td></td> </tr> </table>	$a = 750$	$d = 100$	$b = 10$	$e = 0.2$	$c = 250$	
$a = 750$	$d = 100$							
$b = 10$	$e = 0.2$							
$c = 250$								
Fa	a = speed of movement [mm/min]							
G91								
M98 p1236 lb	b = number of layers							
M30								
O1236	$c = [d/2*e]$; number of repetitions							
M98 p1237 lc								
G1 xd								
G1 y-d								
M98 p1238 lc								
O1237	d = scaffold dimensions in X and Y [mm]							
G1 xd								
G1 ye	e = interfilament space [mm]							
G1 x-d								
G1 ye								
M99								
O1238								
G1 y-e								
G1 xd								
G1 y-e								
G1 x-d								
M99								
M2	END OF PROGRAM							
CODE	EXPLANATION	ILLUSTRATION						
G17 G21 G40 G49 G54 G80 G94	START OF PROGRAM	 <p>diameter depending on implemented mandrel</p> <p>example values for a tubular scaffold of 50mm in length</p> <table border="1"> <tr> <td>$a = 500$</td> <td>$c = 200$</td> </tr> <tr> <td>$b = 800$</td> <td>$d = 50$</td> </tr> </table>	$a = 500$	$c = 200$	$b = 800$	$d = 50$		
$a = 500$	$c = 200$							
$b = 800$	$d = 50$							
Fa	a = speed of movement [mm/min]							
G91								
Rb	b = rotational speed [rad/min]							
G98								
M98 p1236 lc	c = number of repetitions in X [mm]							
M30								
O1236	d = scaffold dimensions in X [mm]							
G1 xd								
G1 x-d								
M99								
M2	END OF PROGRAM							

Table 2: Explanation of programming a G-Code for flat and tubular scaffolds, using a text file (.txt) to be uploaded in the software. Please click here to view a larger version of this table.

	Small scales (3 μ m - 10 μ m)	Medium scales (10 μ m - 20 μ m)	Large scales (20 μ m - 30 μ m)
Air pressure [bar]	1 1.5 2 2.5 3 	1 1.5 2 2.5 3 	1 1.5 2 2.5 3
Voltage [kV]	2 4 6 8 10 12 	2 4 6 8 10 12 	2 4 6 8 10 12
Collection speed [mm/min]	400 800 1200 1600 2000 	400 800 1200 1600 2000 	400 800 1200 1600 2000
Results			
Explanation	Reduced pressure initiates less mass extrusion. Less electrostatic force needed to accelerate fiber. High collection speed initiates enhanced stretching.	Increased pressure leads to more mass flow. Enhanced applied voltage needed to drag polymer. Medium collection speed to not overstretch jets.	High pressure extrudes large amounts of material. High voltage needed for stabilization. Low collection speed for minimal fiber stretching.

Table 3: Representative values of the parameters air pressure, voltage and collection speed (temperature and collection distance constant) to reach three different diameter ranges (small, medium and large). The red arrows propose exact values within the respective categories to reach the fiber diameters. [Please click here to view a larger version of this table.](#)

FIBER PATHWAY		ADJUSTMENTS FOR OPTIMIZATION
<p>desired pathway</p>	<p>flight paths resembles constant catenary curve</p> <p>do not change the parameters</p>	
<p>case 1: pulsing</p>	<p>periodically deflecting flight paths</p> <p>decrease air pressure</p> <p>increase speed</p> <p>minimize voltage</p>	
<p>case 2: lagging jet</p>	<p>fiber lags behind</p> <p>reduce air pressure</p> <p>decrease speed</p> <p>increase voltage</p>	
<p>case 3: buckling stream</p>	<p>fiber travels vertically</p> <p>increase air pressure</p> <p>increase speed</p> <p>reduce voltage</p>	

Table 4: Schematic illustration of the different cases and real images of possible fiber deposition at MEW as well as means to optimize. Please click [here](#) to view a larger version of this table.

Discussion

Integrating AM in order to find innovative solutions for the challenges in the medical field presents a new paradigm for the 21st century. The so-called field of "Bio-fabrication" is on the rise and innovations in fabrication technologies enable the production of highly sophisticated architectures for TE applications. The electrospinning of polymer melts in a direct writing mode (here MEW) is seen as one of the most promising manufacturing candidates to comply with the needs of the TE community, where ordered structures of biocompatible materials in the micron to nanoscale are required²⁷.

This tutorial aims at generating fundamental knowledge of the operations of MEW by explaining the physical principles and demonstrating action steps to manufacture reproducible scaffolds using this technology.

Since the general principles of MEW are comparable to those of conventional additive manufacturing technologies, i.e. a targeted deposition of extruded material in a layer by layer manner, it is crucial to control the relative movement between the head and the collector. From our experience, we recommend working with MEW devices that keep a fixed head, while the respective movement of the collector is undertaken by the stages (X and Y). A fixed head remains in a stable position and does not generate kinematic forces, which would act on the Taylor cone and potentially lead to disturbances during its creation. In addition, the wiring associated with high voltage and heaters is not subject to sustained repetitive movement. The collector movement is defined by the G-Code, which needs to be uploaded in the software. This code, also known as RS-274, is widely used in the computer-aided manufacturing field to control the pathway of tools. For MEW applications with flat collectors, the G-Code file determines the movement and speed in X and Y direction; for cylindrical collectors or mandrel applications, the G-Code file defines both the translational (X direction) and rotational speeds. **Table 2** explains the programming of a G-code in more detail.

Compared to other additive manufacturing technologies, MEW enables the fabrication of fibers with various diameters by the adjustment of the system parameters temperature, collection speed and applied voltage, as described in the protocol.

In order to achieve small fibers (3-10 μm), it is advised to use low pressures, moderate voltages and high collection speeds. Generally, reduced pressure leads to less extruded mass. This is accompanied by a corresponding decrease in the surface area of the jet. Hence, smaller electrostatic forces are required to accelerate the mass of the fiber towards the collector, i.e. lower voltage needs to be applied. Additionally, comparable higher collection speeds lead to enhanced stretching of the fiber, causing an additional reduction of the final fiber diameter.

Increasing the pressure induces more flow of molten polymer and thus, leads to larger fiber diameters (10-20 μm). In this case, greater electrostatic force is required to compensate for the enlarged polymer surface (thicker fibers). In order to obtain a stable polymer jet stream, voltage must be altered and the collection speed should be reduced.

Large fiber diameters (20-30 μm) require enhanced polymer extrusion, i.e. higher air pressure. This provokes relatively thicker fibers and is suggested to be applied in combination with higher voltage to supply sufficient electrostatic force on the fiber. Additionally, reduced collecting speeds induce less fiber stretching. A summary is given in **Table 3**.

All three cases mentioned above, however, still require fine-tuning and optimization to maintain a stable catenary curve shaped fiber over time, explained in the protocol. In MEW, only a perfectly balanced equilibrium between the forces determining the flow of the polymer mass and the forces attracting the jet towards the collector will eventually lead to reaching consistent scaffold morphologies^{12,28}. Hence, divergences of the pathway of the jet reflect strong deviations of the fiber diameter or inaccurate deposition. From our experience, three different variations in behavior can be obtained.

First, a fiber can pulse, a phenomena initially reported by the Dalton group¹². An unbalanced distribution between delivered mass and respective drag-forces on the fibers results in a constantly overfed Taylor cone, which periodically releases accumulated polymer. This causes significant variability in the angles of the pathway and results in differing diameters.

Second, a lagging electrified jet occurs when the speed of the collector is higher than the extrusion speed of the jet. The final deposition of the jet happens far away from the vertical direction of the spinneret, causing a lagging jet stream. The flight path resembles an overemphasized curvature, which also minimizes the dimensions of a printed scaffold.

Third, a buckling electrified jet is caused by the perpendicular impact of the jet onto the collector and manifests, when the collector speed is set slower than the speed at which the jet is flowing out of the spinneret. Applying high voltages can also cause buckling, by producing an excessive acceleration towards the collector and a straight flight path of the fiber. Undesired deposition of loops is observed in this case.

Means to re-stabilize the process are provided in the protocol and shown in **Table 4**.

From the perspective of scaffold implementation, multiple benefits exist when using PCL and MEW, such as biocompatibility, reproducibility through direct writing, or predesigned customization of the resulting architectures. MEW can be conducted on any conventional laboratory bench, since it uses solvent-free polymer melts, therefore it does not require expensive fume hoods or exhaustive recycling of residual materials²⁹. There is no odor when entering a room containing MEW devices.

Additionally, an achievable high surface to volume ratio within a porous scaffold is of great advantage and makes MEW scaffolds well suited for biological applications³⁰.

In comparison to well-known 3D printing technologies, such as Fused Deposition Modelling³¹, MEW has limitations in printable heights of ordered structures. The reason is seen in the inherent process of applying electrostatic forces, which traps mobile charge carriers within the deposited fibers. Once the height of scaffolds exceeds approximately 4 mm, it is reported that the sum of the excess charge accumulated within the scaffold acts repelling for upcoming fibers³². Subsequently, in most cases, the resulting top layers are significantly distorted.

Another difference to conventional 3D printing technologies lies in the fact that the deposition of material during the process cannot be interrupted and solely stopping all system parameters eventually holds material extrusion. This represents a design limitation and must be regarded when programming the G-Code. While the jet initiation can be performed mechanically³³, G-Code programming needs to consider a continuous direct-writing approach.

Increasing the throughput and process efficiency of MEW also remains a challenge and represents the main reason in our view and others' of why this technology has not been up-scaled to industrial level yet³⁴. First, the MEW process is inherently low in throughput due to the low flow rates and limited collection speeds. Both aspects, however, are essential to ensure the controlled deposition of the jet and reproducibility in the printing. Indeed, the maximum collection speed during the printing process is restricted to the physical boundaries of the material used, i.e. too high speeds would cause breakage of the jet when the drag forces exceed feasible limits. Another strategy to upscale relies on using multi-extruding MEW devices, i.e. machines with multiple printing heads in close distance to each other; however, these multi-heads would cause interferences between the electrical field of each head, and subsequently distort the final fiber deposition³⁵. Needleless melt electrospinning heads have generated a significant number of electrified jets³⁶, although controlling the exact placement of the direct-written fibers could be difficult to achieve. Future developments towards increasing the efficiency of MEW, however, would not only benefit the biomedical community, but also the industries of filtration, textile, or applications for energy².

Although this tutorial provides guidelines to fabricate customized scaffolds under the proposed parameter settings, it must be noted that minor dependencies on environmental conditions, such as room temperature or humidity exist and might lead to unintended deviations³⁷. The results presented in this tutorial are based on know-how accumulated at the Hutmacher group, conducted in stable environmental conditions within controlled laboratory spaces.

PCL is the most prominent candidate for MEW. From an engineering perspective, its low melting point (60 °C) is beneficial as this does not require the challenging implementation of high temperature heaters (>>100 °C) in close distance to high voltage sources. On a material engineering level, PCL is semi-conductive and provides strong macromolecular cohesion both as a fluid and as a solid. Despite strong mechanical stretching, the viscous material bonds to a certain degree, which results in prominent fiber thinning when increasing collector speed or applied voltage. Conventional melt electrospinning without moving collectors has been reported with different polymers, such as polypropylene, polyethylene or nylon⁹. The application of direct writing principles however, has predominantly been reported with PCL and some PCL blends with additives to further lower its viscosity³⁸, although there are exceptions^{39,40}. In the future, however, we foresee a wider range of materials processed by MEW. This, in turn, will imply the upgrade of hardware components for this technology, as for example processing polypropylene (melting point at 160°C) alters the current technical requirements of the hardware of MEW devices.

An increasing interest in biocompatible polymeric scaffolds with highly precise and controllable architectures exists; MEW, to date, represents the only technology, which, in comparison to other biomufacturing techniques, is capable of fabricating ordered architectures in the lower micron range (with exceptions in the sub-micron range⁴¹). Within the last years this lead to an exponentially growing amount of patents and publications³⁰. Therefore, tackling technical complexity through implementation of optimized hardware and the establishment of in-process control of MEW is of great importance. This will facilitate the production of scaffolds with tailored architectures for a wide range of applications in the future.

Disclosures

The authors have nothing to disclose.

Acknowledgements

This work has been financially supported by the Cooperative Research Centre CRC for Cell Therapy Manufacturing, the Australian Research Council ARC Centre in Additive Biomufacturing and the Institute for Advanced Study of the Technical University of Munich. This research was conducted by the Australian Research Council Industrial Transformation Training Centre in Additive Biomufacturing <http://www.additivebiomufacturing.org> (IC160100026). Please visit the site for articles, books, television or radio programs, electronic media, or any other literary works related to the Project. Further, the authors gratefully acknowledge Maria Flandes Iparraguirre for support in filming, Philip Hubbard for the voice over and Luise Grossmann for filming and editing.

References

- Muerza-Cascante, M. L., Haylock, D., Hutmacher, D. W., & Dalton, P. D. Melt Electrospinning and Its Technologization in Tissue Engineering. *Tissue Eng Part B Rev.* **21** (2), 187-202 (2015).
- Brown, T. D., Dalton, P. D., & Hutmacher, D. W. Melt electrospinning today: An opportune time for an emerging polymer process. *Prog. in pol. Sci.* (2015).
- Brown, T. D., Dalton, P. D., & Hutmacher, D. W. Direct writing by way of melt electrospinning. *Adv Mater.* **23** (47), 5651-5657 (2011).
- Farrugia, B. L. *et al.* Dermal fibroblast infiltration of poly(ϵ -caprolactone) scaffolds fabricated by melt electrospinning in a direct writing mode. *Biofabrication.* **5** (2), 025001 (2013).
- Brown, T. D. *et al.* Melt electrospinning of poly (ϵ -caprolactone) scaffolds: Phenomenological observations associated with collection and direct writing. *Mater. Sci. Eng. C.* **45** 698-708 (2014).
- Jungst, T. *et al.* Melt electrospinning onto cylinders: effects of rotational velocity and collector diameter on morphology of tubular structures. *Polym Int.* **64** (9), 1086-1095 (2015).
- Brown, T. D. *et al.* Design and Fabrication of Tubular Scaffolds via Direct Writing in a Melt Electrospinning Mode. *Biointerphases.* **7** (1), 1-16 (2012).
- Woodruff, M. A., & Hutmacher, D. W. The return of a forgotten polymer-Polycaprolactone in the 21st century. *Prog. in pol. Sci.* **35** (10), 1217-1256 (2010).
- Hutmacher, D. W., & Dalton, P. D. Melt electrospinning. *Chem Asian J.* **6** (1), 44-56 (2011).
- Wei, C., Gang, T.-Q., Chen, L.-J., & Zhao, Y. Critical condition for the transformation from Taylor cone to cone-jet. *Chin. Phys. B.* **23** (6), 064702 (2014).
- Mikl, B. *et al.* Discrete viscous threads. *ACM Trans. Graph.* **29** (4), 1-10 (2010).
- Hochleitner, G. *et al.* Fibre pulsing during melt electrospinning writing. *BioNanoMaterials.* **17** (3-4), 159 (2016).
- Poh, P. S. P. *et al.* Polyactides in additive biomufacturing. *Adv Drug Del Rev.* **107** 228-246 (2016).
- Vaquette, C., & Cooper-White, J. J. Increasing electrospun scaffold pore size with tailored collectors for improved cell penetration. *Acta Biomater.* **7** (6), 2544-2557 (2011).
- Thibaudeau, L. *et al.* A tissue-engineered humanized xenograft model of human breast cancer metastasis to bone. *Dis Model Mech.* **7** (2), 299-309 (2014).
- Holzappel, B. M. *et al.* Species-specific homing mechanisms of human prostate cancer metastasis in tissue engineered bone. *Biomaterials.* **35** (13), 4108-4115 (2014).
- Bas, O. *et al.* Enhancing structural integrity of hydrogels by using highly organised melt electrospun fibre constructs. *Eur. Polym. J.* **72** 451-463 (2015).
- Visser, J. *et al.* Reinforcement of hydrogels using three-dimensionally printed microfibres. *Nat. Commun.* **6** 6933 (2015).
- Haigh, J. N. *et al.* Hierarchically Structured Porous Poly(2-oxazoline) Hydrogels. *Macromol. Rapid Commun.* **37** (1), 93-99 (2016).
- Wagner, F. *et al.* A validated preclinical animal model for primary bone tumor research. *JBJS.* **98** (11), 916-925 (2016).
- Baldwin, J. *et al.* Periosteum tissue engineering in an orthotopic in vivo platform. *Biomaterials.* **121** 193-204 (2017).
- Tourlomis, F., & Chang, R. C. Dimensional Metrology of Cell-matrix Interactions in 3D Microscale Fibrous Substrates. *Procedia CIRP.* **65** 32-37 (2017).
- Muerza-Cascante, M. L. *et al.* Endosteal-like extracellular matrix expression on melt electrospun written scaffolds. *Acta Biomater.* **52** 145-158 (2017).
- Delalat, B. *et al.* 3D printed lattices as an activation and expansion platform for T cell therapy. *Biomaterials.* **140** 58-68 (2017).
- Bas, O. *et al.* Biofabricated soft network composites for cartilage tissue engineering. *Biofabrication.* **9** (2), 025014 (2017).
- Hansske, F. *et al.* Via precise interface engineering towards bioinspired composites with improved 3D printing processability and mechanical properties. *J. Mater. Chem. B.* (2017).
- Melchels, F. P. W. *et al.* Additive manufacturing of tissues and organs. *Prog. in pol. Sci.* **37** (8), 1079-1104 (2012).
- Hochleitner, G. *et al.* Fibre pulsing during melt electrospinning writing. *BioNanoMaterials.* Vol. 17 159 (2016).

29. Persano, L., Camposeo, A., Tekmen, C., & Pisignano, D. Industrial Upscaling of Electrospinning and Applications of Polymer Nanofibers: A Review. *Macromol. Mater. Eng.* **298** (5), 504-520 (2013).
30. Wunner, F. M. *et al.* in *Comprehensive Biomaterials II*. 217-235 Elsevier, (2017).
31. Loh, Q. L., & Choong, C. Three-Dimensional Scaffolds for Tissue Engineering Applications: Role of Porosity and Pore Size. *Tissue Eng Part B Rev.* **19** (6), 485-502 (2013).
32. Ristovski, N. *et al.* Improved fabrication of melt electrospun tissue engineering scaffolds using direct writing and advanced electric field control. *Biointerphases.* **10** (1), 011006 (2015).
33. Wei, C., & Dong, J. Direct fabrication of high-resolution three-dimensional polymeric scaffolds using electrohydrodynamic hot jet plotting. *J Micromech Microeng.* **23** (2), 025017 (2013).
34. Hacker, C. *et al.* Electrospinning of polymer melt : steps towards an upscaled multi-jet process. *Proceedings of the International Conference on Latest Advances in High Tech Textiles and Textile-Based Materials*. 71-76 (2009).
35. Nayak, R., Padhye, R., Kyratzis, I. L., Truong, Y. B., & Arnold, L. Recent advances in nanofibre fabrication techniques. *Text. Res. J.* **82** (2), 129-147 (2012).
36. Li, H. *et al.* Interjet distance in needleless melt differential electrospinning with umbellate nozzles. *J. Appl. Polym. Sci.* **131** (15) (2014).
37. Liao, S. *et al.* Effect of humidity on melt electrospun polycaprolactone scaffolds. *BioNanoMaterials*. Vol. 17 173 (2016).
38. Detta, N. *et al.* Melt electrospinning of polycaprolactone and its blends with poly(ethylene glycol). *Polym Int.* **59** (11), 1558-1562 (2010).
39. Hochleitner, G., Hümmer, J. F., Luxenhofer, R., & Groll, J. High definition fibrous poly(2-ethyl-2-oxazoline) scaffolds through melt electrospinning writing. *Polymer.* **55** (20), 5017-5023 (2014).
40. Chen, F. *et al.* Additive Manufacturing of a Photo-Cross-Linkable Polymer via Direct Melt Electrospinning Writing for Producing High Strength Structures. *Biomacromolecules.* **17** (1), 208-214 (2016).
41. Hochleitner, G. *et al.* Additive manufacturing of scaffolds with sub-micron filaments via melt electrospinning writing. *Biofabrication.* **7** (3), 035002 (2015).